Ibn Al-Haitham Journal for Pure and Applied Sciences
Journal homepage: jih.uobaghdad.edu.iq
PISSN: 1609-4042, EISSN: 2521-3407
IHJPAS. 2026; 39(2)

Nanoscale Processing of Euphrates Poplar for Methylene Blue Removal

Sara Mohammed Hassan[1*], and Ahlam Mohammed Farhan[2]
[1,2] Department of Chemistry, College of Science for Women, University of Baghdad, Baghdad, Iraq
*Corresponding Author

Received: 28/October/2025
Accepted: 18/January/2026
Published: 20/April/2026
doi.org/10.30526/39.2.4314

Abstract

The potential of Euphrates poplar (EP) leaves, a plentiful agricultural waste, as a sustainable adsorbent for wastewater treatment is examined in this work. FTIR, FESEM, and XRD were used to characterize activated carbon (AC) derived from EP leaves by carbonizing them at 400°C for 3 hours. Brunauer found a surface area of 3.77 m^2/g using the Brunauer–Emmett–Teller (BET) technique. Methylene blue (MB) adsorption trials showed that with an ideal contact time of 60 minutes, the removal efficiency exceeded 91%. Temperature and pH significantly affected the adsorption process, and the addition of EP nanoparticles enhanced dye uptake. According to kinetic modeling, the Temkin isotherm (R^2= 0.904) provided the most accurate equilibrium fit, while the pseudo-second-order model (R^2= 0.999) best explained the adsorption behavior. Positive $\Delta S°$ values indicated greater unpredictability at the solid-solution interface, and thermodynamic parameters confirmed that the adsorption was endothermic and spontaneous. These results demonstrate that Euphrates poplar leaves are an economical and environmentally beneficial adsorbent for dye removal, providing a viable alternative for wastewater treatment applications.

Keywords: Adsorption, Euphrates poplar, Kinetics, Methylene blue, Thermodynamics, Wastewater treatment.

1. Introduction

Recent decades have seen a sharp rise in pollutants and hazardous emissions due to rapid industrial innovation, with detrimental effects on the environment[1]. Synthetic dyes are among the most dangerous contaminants due to their widespread use in the food, paper, plastics, and textile sectors. The dye business has grown significantly since Perkins' groundbreaking contributions to organic chemistry in the late 19th century, and today synthetic dyes make up around 90% of the colors used globally[2]. They pose a significant threat to the environment and public health due to their persistence, complex aromatic structures, and ecotoxicity[3]. The harmful effects of dyes and their breakdown products, including their mutagenic and endocrine-disrupting properties, have been the subject of numerous studies. Furthermore, other contaminants, including heavy metals and catalysts, are often used during the dye manufacturing process, exacerbating environmental risks. Advanced oxidation processes, photolysis, and adsorption are among the treatment techniques investigated to remove color from wastewater[4]. Among them, adsorption has proven to be one of the most economical and successful methods, especially for cationic dyes. Because of their inherent functional groups and porous architectures, plant-derived adsorbents have been shown to improve adsorption efficiency[5]. Despite these developments, a substantial number of current adsorbents rely on expensive activated carbon or tailored nanomaterials, which, although efficient, are not sustainable or financially viable for large-scale applications. Additionally, locally available biomass resources that could serve as environmentally beneficial substitutes have received little attention. Adsorbents that combine high efficiency with affordability, sustainability, and ease of preparation remain in demand. One interesting option for dye

adsorption is the Euphrates poplar (Populus euphratica), a plant that grows naturally along riverbanks[6]. Its lignocellulosic composition offers opportunities for pollutant removal, in addition to its ecological functions as a wind barrier and soil stabilizer. The goal of this research is to develop an economical and practical adsorbent material from Euphrates poplar for the removal of methylene blue (MB) and related dyes from aqueous solutions. It will specifically examine how operational factors affect adsorption efficiency, including temperature, initial dye concentration, adsorbent dosage, pH, and contact time[7,8]. This study aims to demonstrate that Euphrates poplar is a feasible substitute for wastewater treatment, promoting environmental preservation and sustainable resource use, by benchmarking against published research and comparing it with current adsorbents. This study is novel since Euphrates poplar (Populus euphratica) leaves have not been extensively studied as biosorbents for dye removal. This underutilized agricultural waste, abundant in riparian environments, provides a low-cost, sustainable alternative to commercial activated carbon and nanomaterials. Using kinetic, isothermal, and thermodynamic analyses, the current study assesses its adsorption capacity under various operational conditions. Euphrates poplar is a viable option for wastewater treatment because of these characteristics.

2. Materials and Methods

2.1. Preparation of nano Euphrates poplar (EP) leaf powder

The synthesis of nanoparticles (NPs) from Euphrates extract requires a well-coordinated series of processes to produce fine particles suitable for a variety of applications. Purification begins with a crisscross approach along the Euphrates River to remove impurities, including dust and biological contaminants. During the cleaning procedure, the samples may be subjected to a controlled, brief heating treatment, which can be done either outside or in a private laboratory. Since temperature management is crucial for preserving functional materials, the choice of cooling technique depends on the experiment's needs and the preservation of biologically active compounds. After drying, the Euphrates poplar leaves were ground with high-performance, rapid grinders to obtain a homogeneous powder. The powder was then sieved using a 75-µm mesh. A 10 g sample of the powder was weighed and treated by adding 100 mL of 0.1 M hydrochloric acid to the resulting mixture, followed by continuous stirring for 2.5 hours with a magnetic stirrer at 30°C. Subsequently, 100 mL of 0.1 M sodium hydroxide solution was gradually added while stirring was maintained for an additional half hour. The solution was then filtered to separate the precipitate, which was dried for 2 hours at 150 °C in an oven. This was followed by calcining the dried precipitate at 400°C for 3 hours, yielding a highly efficient nanopowder, as shown in **Scheme 1**.

2.2. Preparation of absorbed solutions

Methylene blue dye was used to prepare a solution to study the efficiency of a previously prepared surface in adsorbing the dye. The dye has the following molecular formula: ($C_{16}H_{18}N_3SCl.3H_2O$). The stock solution of MB (0.1 g) was prepared using distilled water. The stock solution was further diluted to concentrations of 10, 20, 30, 40, 50, 70, 80, 90, and 100 mg/L using distilled water.

2.3. Batch adsorption of MB dye on nano Euphrates poplar leaf powder (EP)

The equilibrium isotherm curve of a well-characterized adsorbent illustrates its intrinsic adsorption properties. In the experiment, a 50 ppm MB dye solution was prepared using deionized water[9]. A 10 mL aliquot of this dye solution was combined with 0.4 g of nano-treated Euphrates poplar leaf powder and heated at 298 K for 60 minutes. Following filtration, the dye concentration in the solution was determined utilizing a UV-Vis absorption spectrometer[10], as shown in **Equation 1**.

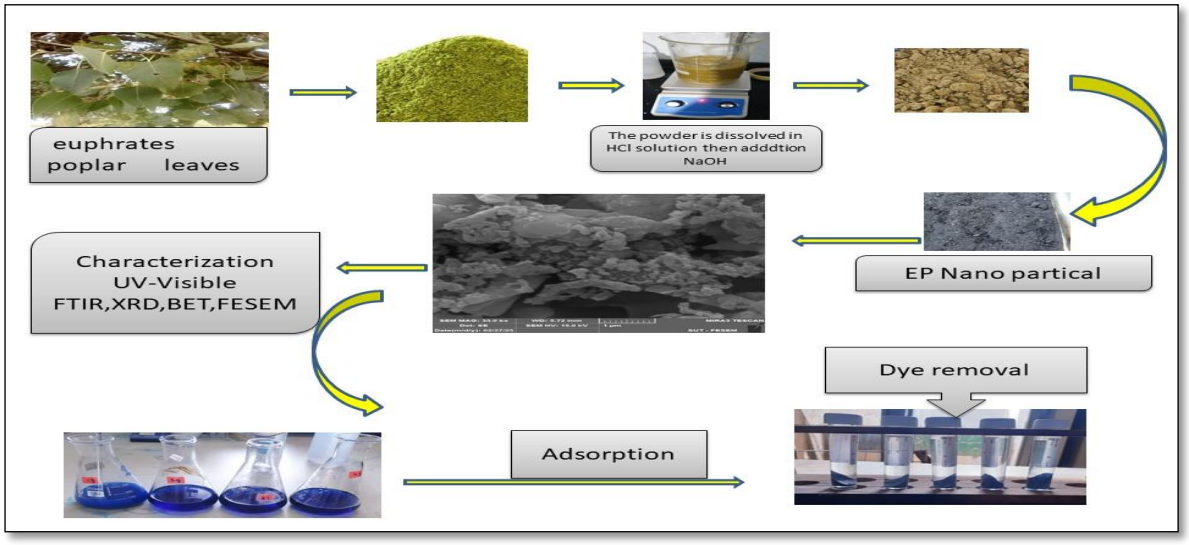

Scheme 1. Adsorption pathway of MB on activated carbon/EP

2.4. Statistical analysis

The data obtained from the experiment were utilized for statistical analysis. All trials were conducted in triplicate, and the findings are given as mean standard deviation. To assess statistical significance, SPSS was used with a predetermined significance level ($p < 0.05$).

3. Results

The features of EP NPs were carefully studied using Fourier transform infrared (FTIR) spectroscopy, which provided critical information on their molecular structure and chemical composition. An X-ray diffractometer (XRD-6000) was employed to facilitate this process and enable a more comprehensive study. The shape and surface details of the NPs were studied using scanning electron microscopy (SEM), providing a comprehensive view of their structure. Furthermore, this study assessed its qualitative surface area using the Brunauer–Emmett–Teller (BET) method, ensuring precise and thorough data acquisition, as shown in **Tables 1-3** and **Figures 1-7**.

Table 1. Parameters of MB adsorption models onto EP at 298-328 K

T (k)	Langmuir Constant			Freundlich Constant		Temkin Constant	
	q_{max}	K_L	R_L	n	K_f	K_T	b
298	0.12	0.359	0.357	2.288	5.4	3.739	860.3
308	0.085	0.4	0.0476	2.27	5.27	3.55	522.9
318	0.26	0.135	0.129	2.4	4.9	3.589	466.28
328	0.286	0.13	0.133	2.5	4.78	2.846	1056.97

Table 2. Rate constant values for reactions following pseudo-first and pseudo-second-order kinetics

Pseudo-First order			Pseudo-Second order		
K_1	q_e	R^2	K_2	q_e	R^2
0.0126	0.01238	0.7083	0.849	1.093	0.9999

Table 3. Thermodynamic parameters for the adsorption of MB on the EP surface at 298-328 K

C_0 (ppm)	T(k)	ΔH (KJ/mol)	ΔG (KJ/mol)	ΔS (J/K.mol)
10	298 308 318 328	1.5122	-0.3289 -0.5978 -1.301 -1.51	9.214
20	298 308 318 328	1.00579	-3.2124 -3.62 -3.895 -4.398	16.5
30	298 308 318 328	0.681	-4.073 -4.901 -4.798 -5.174	17.85
40	298 308 318 328	0.85542	-4.707 -5.339 -5.684 -5.863	20.483
50	298 308 318 328	1.1268	-5.16 -5.53 -6.252 -6.521	23.316

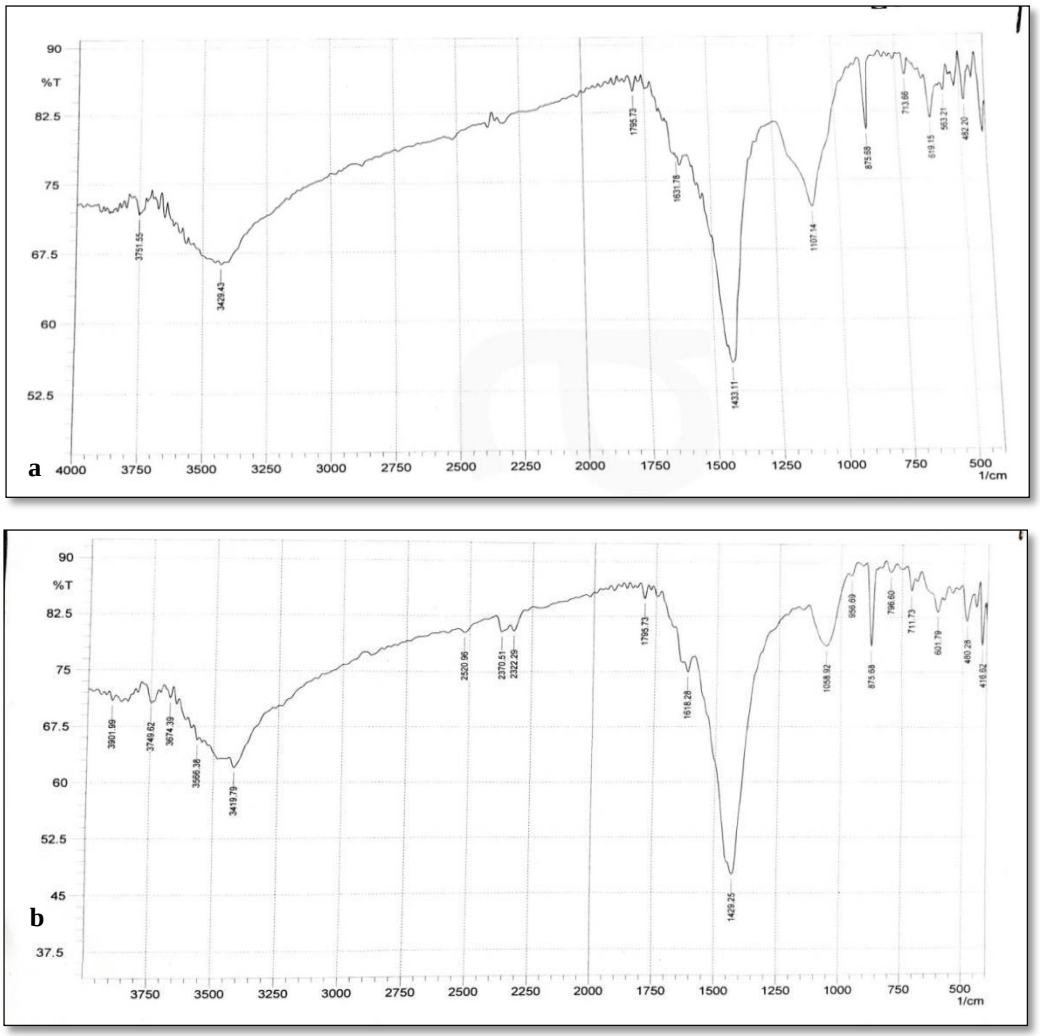

Figure 1. FTIR spectroscopy of EP NPs (a) Before adsorption (b) After adsorption

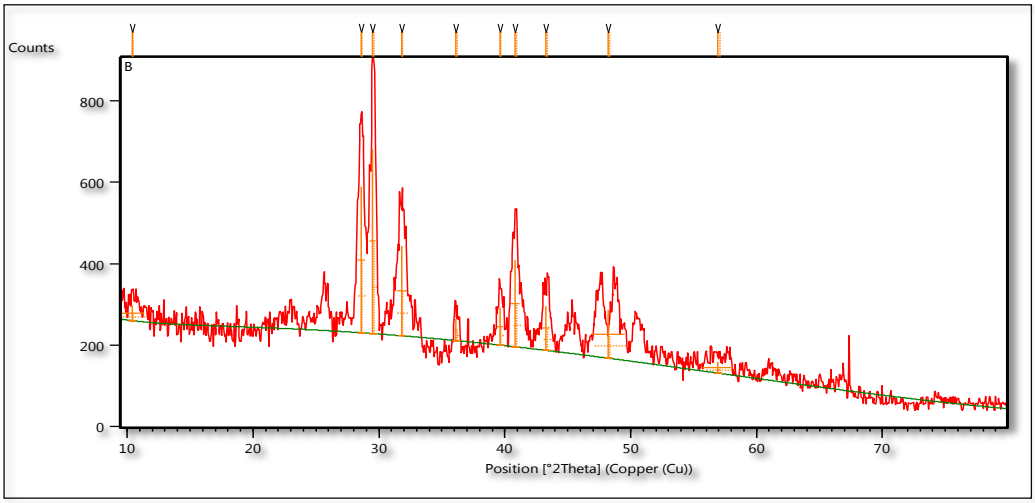

Figure 2. XRD patterns of EP NPs

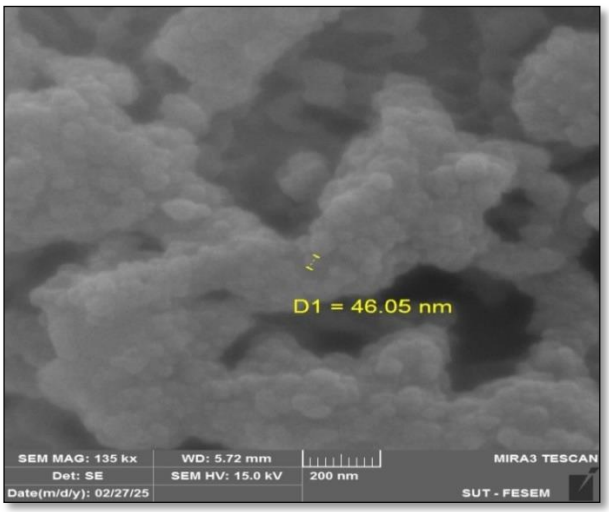

Figure 3. FESEM of EP NPs

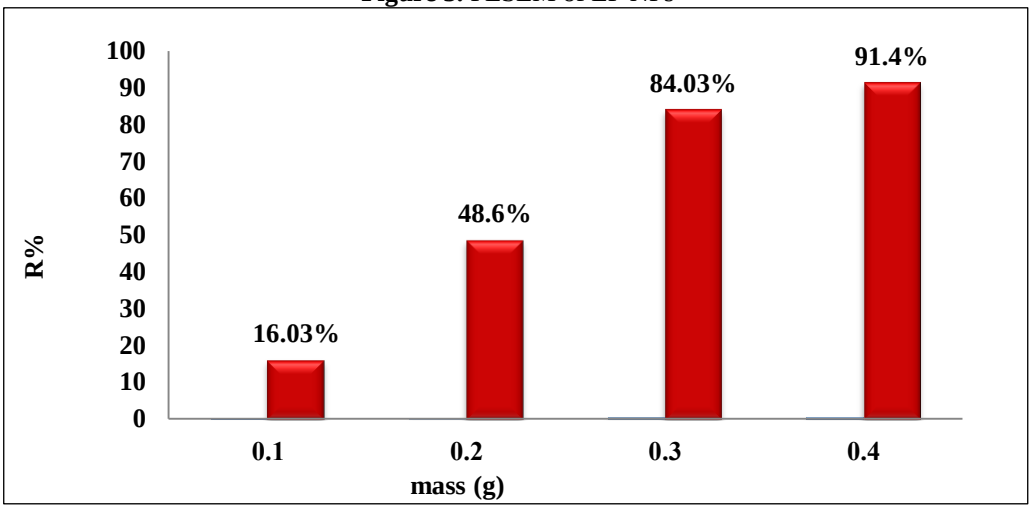

Figure 4. Effect of adsorbent dose on the percent of dye removal on the EP

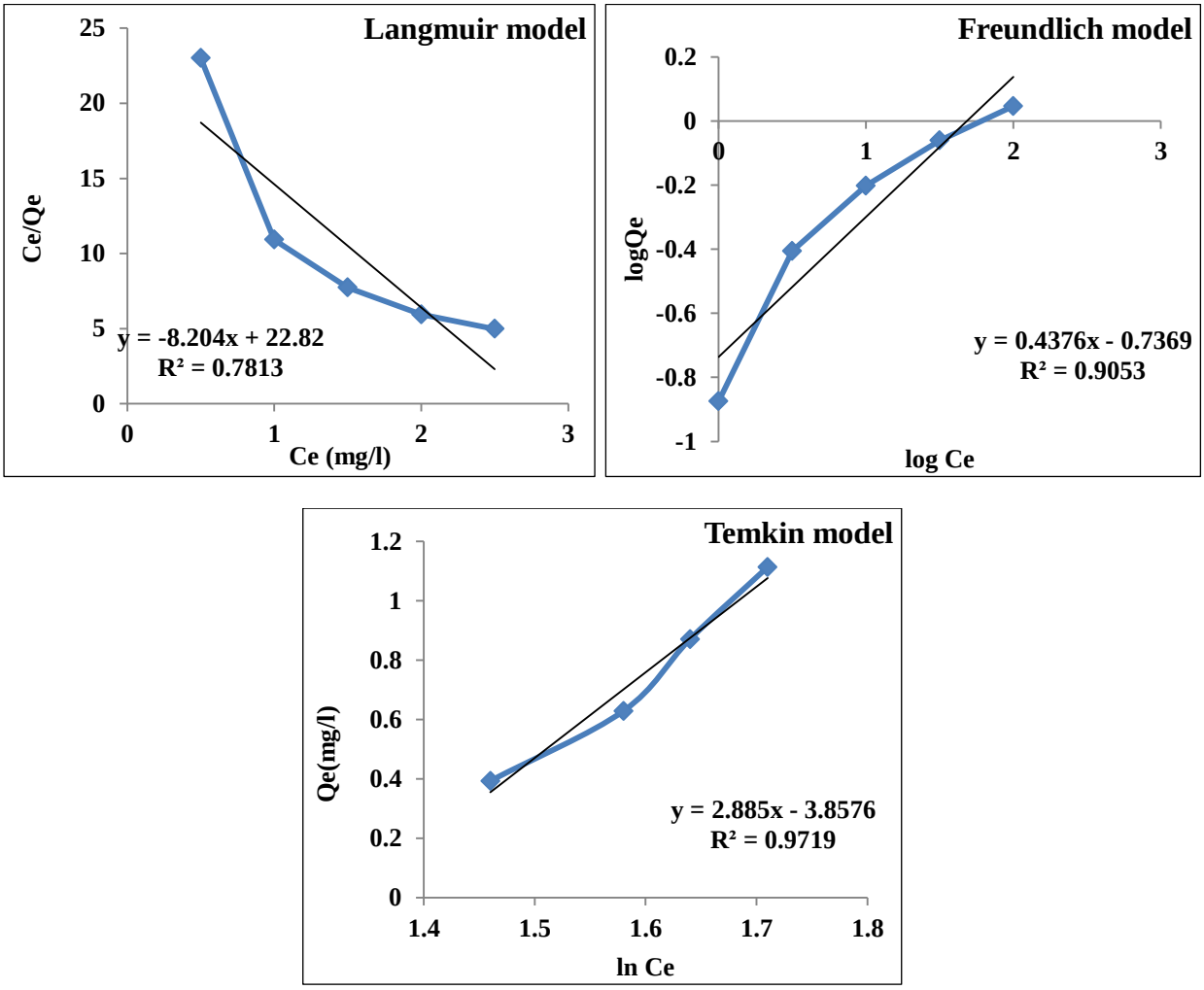

Figure 5. Isotherms model (Langmuir, Freundlich, and Temkin) at 298 K

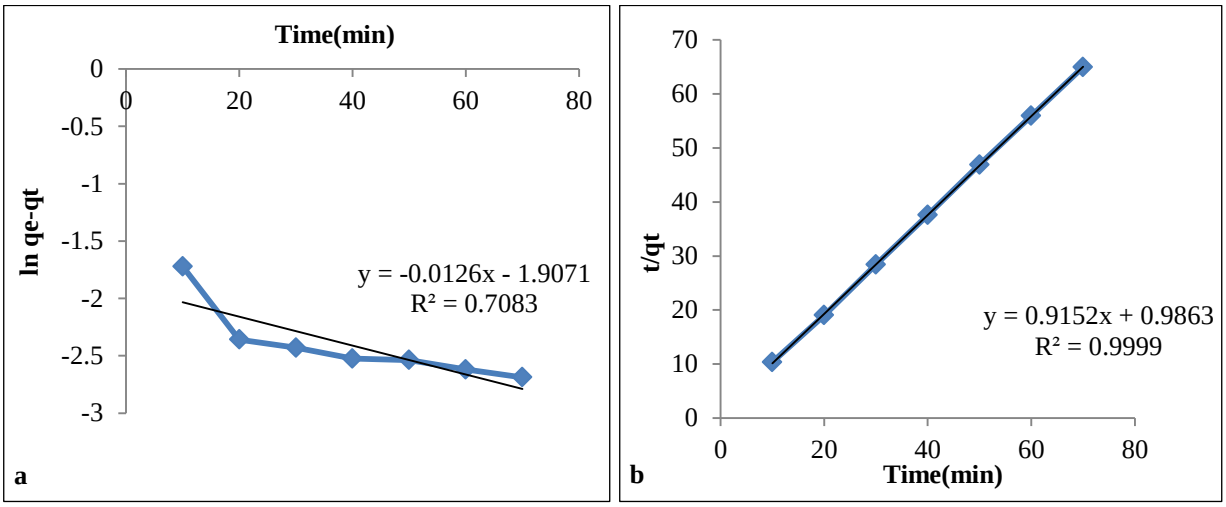

Figure 6. Kinetic adsorption of MB dye. a- Pseudo-first-order, b- Pseudo-second-order

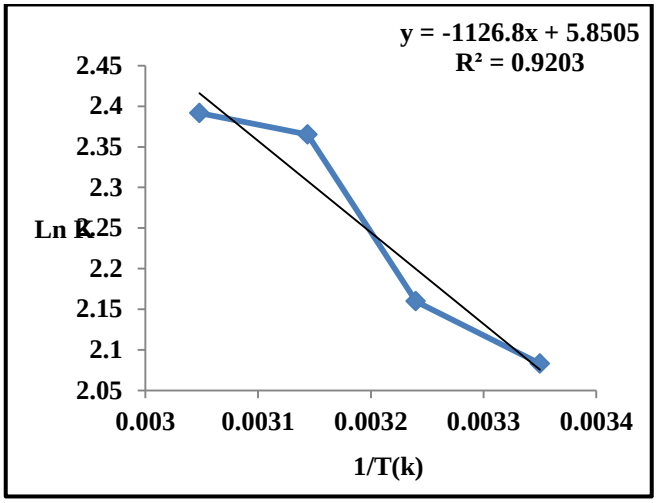

Figure 7. The relationship between ln K and 1/T(k) in the Van't Hoff

Langmuir, Freundlich, and Temkin models are demonstrated in the following **Equations**:

$$Qe = (C0 - Ce)\, Vsol/m \quad \textbf{(1)}$$

C_0 and Ce represent the initial and equilibrium concentrations of MB dye (mg/L), respectively. Qe (mg/g) denotes the equilibrium adsorption capacity. M is the mass of the Euphrates poplar leaf powder NPs (g), and Vsol refers to the volume of the methylene.

$$D = k\lambda / \beta cos\theta \quad \textbf{(2)}$$

Here, D represents the particle size in nanometers (nm), k is a constant with a value of 0.94, β is the full-width at half maximum (FWHM) of the peak measured in radians, λ is the X-ray wavelength (1.5406 Å), and 2θ corresponds to the Bragg angle in degrees.

$$Ce/Qe = 1/q\,max\,Kl + Ce/q\,max \quad \text{Langmuir} \quad \textbf{(3)}$$

$$log(Qe) = log(kg) + \left(\frac{1}{n}\right) log(Ce) \quad \text{Freundlich} \quad \textbf{(4)}$$

$$Qe = \frac{RT}{b} LnA\ \text{Ce} \quad \text{Temkin} \quad \textbf{(5)}$$

$$\ln(\text{qe} - \text{qt}) = \ln(\text{qe}) - \text{k1 t} \quad \textbf{(6)}$$

$$/\text{qt} = 1/\text{k2 qe} + \text{t}/\text{qe} \quad \textbf{(7)}$$

$$Ln(Ke) = -\Delta H/RT + \Delta S/R \quad \textbf{(8)}$$

Where R is the universal gas constant (R =8.314 $kJ/kmol.K$), T is the absolute temperature of the solution (K), and Ke is the distribution coefficient that can be calculated by Equation 8.

$$Ke = \frac{Qe}{Ce} \quad \textbf{(9)}$$

$$Ke = qe/Ce \quad \textbf{(10)}$$

Where qe represents the quantity of adsorbed MB per unit weight of activated carbon at equilibrium concentration (mg/g), and Ce denotes the equilibrium concentration of MB (mg/L).

$$\Delta G^{o} = \Delta H^{o} - T\Delta S^{o} \quad \textbf{(11)}$$

4. Discussion

The features of EP NPs were carefully studied using Fourier transform infrared (FTIR) spectroscop[11], providing critical information about their molecular structure and chemical composition. An X-ray diffractometer (XRD-6000) was employed to facilitate this process and enable a more comprehensive study[12]. The shape and surface details of the NPs were studied using scanning electron microscopy (SEM), providing a comprehensive view of their structure. Furthermore, we assessed its qualitative surface area using the Brunauer–Emmett–Teller (BET) method, ensuring precise and thorough data acquisition[13-15].

4.1. FTIR spectroscopy

Fourier transform infrared spectroscopy enables examination of changes in surface functional groups on Euphrates poplar leaves before and after MB absorption. This allows the identification of the active sites responsible for adsorption.

4.1.1. Qualitative analysis before adsorption

The FTIR spectrum of untreated Euphrates poplar leaf surfaces reveals characteristic absorption peaks at 3751 and 3429 cm^{-1}, indicating O–H stretching vibrations in alcohols or phenols, which suggest the presence of O–H groups involved in hydrogen bonding. 1631 cm^{-1}, associated with C=C vibrations in aromatic rings or N–H bending vibrations in amines. 1107 cm^{-1}, representing C–O vibrations in alcohols or ethers. Additional peaks at 875, 713, 619, 563, and 482 cm^{-1}, corresponding to vibrations of aromatic functional groups and low-frequency groupings.

4.1.2. Qualitative analysis after adsorption

Significant spectral changes occur after the adsorption process. A shift of the peak from 3429 cm^{-1} to 3418 cm^{-1} suggests the involvement of O–H groups through hydrogen bonding or changes in their bonding environment. A shift of the peak from 1631 cm^{-1} to 1618 cm^{-1} indicates interactions between C=C or N–H groups and the dye. A shift of the peak from 1107 cm^{-1} to 1058 cm^{-1} indicates changes in C–O bonds, confirming their involvement in interactions with MB.

4.1.3. Emergence of new peaks after adsorption

New peaks that were not present in the original spectrum appear post-adsorption. Key observations include peaks at 3901, 3749, 3674, and 3566 cm^{-1}, likely corresponding to free O–H groups arising from water uptake or surface rearrangement following the reaction. Peaks at 2520, 2370, and 2322 cm^{-1}, potentially linked to C≡N groups or interaction effects such as adsorbed CO_2 from interactions with the dye. Peaks at 796, 955, and 711 cm^{-1}, corresponding to aromatic rings associated with the MB structure. The disappearance of the peak at 563 cm^{-1} suggests direct surface interaction or structural modification resulting from dye adsorption.

The spectral changes demonstrate that the adsorption process involves not just physical surface adherence but also partial chemical reactions. Functional groups such as –OH, C=O, C–O, and C=C actively participate in binding interactions with MB. These findings confirm the potential of Euphrates poplar leaves as a natural adsorbent for removing dyes from aqueous solutions, as shown in **Figure 1**.

4.2.The XRD of EP NPs

The qualitative analysis of the sample revealed that the sample EP pattern aligns entirely with the orthorhombic crystal system of copper oxide (Cu64O, JCPDS No. 01-077-1898). The primary diffraction angles observed for sample B are at 25.73°, 28.54°, 29.54°, 31.79°, 36.16°, 39.65°, 40.89°, 43.31°, 45.51°, 47.66°, 48.80°, 50.56°, 67.02°, and 67.37°. These correspond to the (030), (204), (214), (133), (323), (412), (044), (404), (018), (511), (208), (440), (365), and (634) reflections, respectively. Using the Scherer equation, the average crystallite size of the EP crystal was calculated in **Equation 2**.

Here, D represents the particle size in nanometers (nm), k is a constant with a value of 0.94, β is the full-width at half maximum (FWHM) of the peak measured in radians, λ is the X-ray wavelength (1.5406 Å), and 2θ corresponds to the Bragg angle in degrees. Based on this calculation, the typical crystallite size was computed to be 36.6 nm, as shown in **Figure 2**.

4.3. FE-SEM

Scanning electron microscopy was used to examine the surface morphology of plant powder and the prepared activated carbon. The particle size is tiny (500 nm), which gives the material high structural stability. The pore distribution in this sample is relatively uniform, with smaller pores predominating. **Figure 3** illustrates the geometric configuration and dimensions of the processed material, which is predominantly composed of spherical grains. FESEM analysis revealed that these grains have an average size of 46.05 nm.

4.4. BET

The hypothesis is a scientific approach for determining the surface area of materials by analyzing gas adsorption. This idea is widely used in materials science, is vital for assessing porous structures and determining specific surface areas, and is crucial for processes such as catalysis, adsorption, and filtration. Using the BET approach, researchers can precisely characterize the surface roughness and microstructural features of materials. The test findings reveal that the surface area of EP, as determined by the BET method, is 3.7667 m^2/g. Although a BET surface area of 3.766 m^2/g is low for an adsorbent, effective adsorption can still be achieved through other parameters, especially surface chemistry. In such instances, the type and location of active sites on the surface determine adsorption effectiveness rather than the available surface area.

4.5. Factors influencing adsorption systems

4.5.1. Dosage of adsorbent

Individual pieces of the treated EP powder, each weighing 0.1, 0.2, 0.3, or 0.4 g, were weighed and added to a solution of water containing MB dye. Each sample was immersed in a water bath at 25°C with agitation at 250 rpm for 1 hour. The investigation indicated that 0.4 g of EP powder yielded the highest adsorption effectiveness. The results demonstrate that increasing the adsorbent amount increases the availability of active sites for dye adsorption, thereby boosting the overall efficiency of the process, as shown in **Figure 4**.

4.5.2. Contact time

The time required for MB adsorption on the EP surface to reach equilibrium at 25°C, with a dye concentration of 50 ppm and an adsorbent mass of 0.4 g, was determined. Adsorption was observed to occur rapidly within the first 15 minutes. After this first phase, the adsorption activity decelerated and progressively persisted, ultimately reaching equilibrium after approximately one hour. This behavior can be ascribed to the availability of unoccupied active sites at the start of the process, which promotes rapid adsorption. Over time, as these active sites become occupied by dye molecules, the adsorption rate slows until equilibrium is reached.

4.5.3. Effect of PH

MB dye solutions at pH levels of 3, 5.6, 7, and 10 were prepared, and the adsorption process was conducted under identical conditions. Optimal adsorption performance was observed at pH 5.6. Dye removal from aqueous solutions depends on pH, which affects the adsorbent surface charge, the dissociation degree of the ligand, and the behavior of functional groups attached to the active substance of the EP adsorbent. The maximum adsorption was observed at pH 5.6, with lesser efficacy at pH 3, 7, and 10. This pattern is consistent with how MB and the EP adsorbent's surface interact throughout pH, which is influenced by electrostatics, protonation, and competition for solution species.

4.5.4. Effect of temperature

It has been shown that the quantity of MB eliminated increased with temperature. The MB extraction efficiency of EP surface improved from 88% to 92% as the temperature rose from 25-55°C. The study demonstrated that a rise in temperature is associated with improved MB elimination. This indicates that the elimination of MB is endothermic. When energy levels are adequate, such as at elevated temperatures, the number of molecules interacting with the active site on the surface will increase accordingly[16]. The adsorption efficacy improved at elevated temperatures, as internal diffusion governed the adsorption mechanism. The temperature rise enhances solute transport. Physical activation is more effective at higher temperatures, as it enhances membrane permeability and accelerates cellular activities without the risks of chemical degradation or toxicity[17-20].

4.6. Adsorption isotherms

Adsorption isotherms are graphical representations of the relationship between the amount of a material adsorbed onto a surface and its concentration in the surrounding phase at a constant temperature. These curves are fundamental to understanding adsorption under equilibrium conditions and are widely used in chemistry, environmental science, and materials science. There are several types of adsorption isotherms, each representing distinct adsorption behaviors based

on the nature of the adsorbent, the adsorbate, and their interactions. Standard models include Langmuir isotherms, which assume monolayer adsorption on a homogeneous surface, and Freundlich isotherms, which account for multilayer adsorption and surface heterogeneity. Other advanced models, such as the Temkin isotherm, are used to describe multilayer adsorption in porous materials, as shown in **Equations 3-5**. Understanding these isotherms is crucial for the design and optimization of applications such as catalysis, pollution control, and the development of new materials for industrial processes[21,22].

Figure 5 shows the Freundlich, Langmuir, and Temkin equations, respectively. **Table 1** presents the adsorption constants for the above equations and shows that the adsorption was best described by the Freundlich and Temkin equations, possibly because the adsorption is multi-layer[23]. Based on the R^2 values in **Table 1**, the Freundlich model offers a better fit to the experimental data than the Langmuir model. The n values from the Freundlich model indicate heterogeneous adsorption and positive cooperative interactions. The Langmuir model shows that the maximum monolayer capacity (q_{max}) increases with temperature, implying enhanced adsorption at higher temperatures. Although the Temkin model works well for gas-phase equilibrium, it is less suitable for liquid-phase adsorption. The increase in its b parameter over the 298–328 K range is likely due to stronger interactions between the MB dye and the adsorbent, as well as greater exposure of adsorption sites.

4.7. Kinetic study

The rate of adsorption is contingent upon the mobility of adsorbent particles across the surface of EP particles. Following the experiment, it was determined that dye adsorption on the EP surface reached equilibrium within 1 hour. This adsorption process aligns with a pseudo-second-order kinetic model, as indicated by the correlation coefficient R for this order being superior to that for the pseudo-first-order[24], as shown in **Table 2**. By employing the respective equations for first- and second-order kinetics in **Equations 6** and **7**, the constants for both pseudo-first- and pseudo-second-order models were derived through their linear representations[25-27], as shown in **Figure 6**.

4.8. Thermodynamic parameters

Three thermodynamic variables, namely enthalpy change ΔHo, Gibbs free energy change ΔGo, and entropy change ΔSo, were examined to analyze the thermodynamic behavior of the relationship among the thermodynamic variables enthalpy change ΔHo, entropy change ΔSo, and Gibbs free energy change ΔGo is defined by the Equation[28,29]. The precise assessment of thermodynamic parameters is crucial, as it yields reliable insights into the alterations in potential energy associated with the adsorption process. Key parameters, including the free energy of adsorption (ΔG°), enthalpy (ΔH°), and entropy (ΔS°), were employed to evaluate and interpret subsequent variations, thereby facilitating an accurate estimation of the adsorption mechanism[30], as shown in **Equations 8-10**, and Ke is the distribution coefficient that can be calculated by **Equation 8**.

Where q_e represents the quantity of adsorbed MB per unit weight of activated carbon at equilibrium concentration (mg/g), and Ce denotes the equilibrium concentration of MB (mg/L). The relationship between the thermodynamic parameters, enthalpy change (ΔH°) and entropy change (ΔS°), determines the spontaneity of the adsorption process. Consequently, the alteration in Gibbs free energy, ΔGo[31], is delineated by **Equation 11**.

The Van't Hoff **Equation 10** describes the correlation between ln K and 1/T, where K is the equilibrium constant, and T is the temperature in kelvins, as shown in **Figure 7**. This relationship helps explain how temperature changes influence the position of equilibrium in a chemical reaction. The equation can be expressed in terms of the enthalpy change (ΔH) and entropy change (ΔS) of the response, offering insights into its thermodynamic behavior[32]. From **Table 3**, the adsorption process is endothermic, as evidenced by the positive ΔH values, indicating that it requires heat energy for adsorption to occur. This observation explains why adsorption increases with elevated temperatures, as thermal energy facilitates the process. The negative ΔG values

signify that the adsorption process is spontaneous at the examined temperatures. As the ΔG values decrease with rising temperature, the result indicates that the process becomes increasingly favorable and spontaneous at raised temperatures. Positive values of ΔS indicate an increase in randomness (entropy) during the reaction. In terms of adsorption, this means that after adsorption, the particles on the solid surface and the MB become more randomly arranged[33,34].

5. Conclusion

The investigation demonstrated that the EP plant eliminated MB dye from water. The findings indicate that the plant's physical and chemical characteristics influenced Adsorption. The plant served as an environmentally sustainable and economical adsorbent for MB, effectively decolorizing the dye and reducing its concentration. Adsorption was influenced by physical factors, including plant surface area, functional groups, and particle size. Cellulose, lignin, and the plant's inherent surface charge may have facilitated the adsorption of color. The research indicated that EP effectively eliminated MB dye at a starting dosage of 50 mg. The adsorbent surface weight was 0.4 g, the pH was 5.78, and the contact duration was 60 minutes, achieving a removal efficiency of 92.8%. The correlation coefficient (R^2) indicates that the Freundlich and Temkin models more accurately represent the elimination process of MB dye; however, the Langmuir model is not the most effective isothermal model. Thermodynamic investigation indicates that Adsorption is both spontaneous and endothermic. The slope of the Van't Hoff plot indicated an enthalpy change of 1.1268 kJ/mol, signifying physical Adsorption. The adsorption kinetics followed the pseudo-second-order model, with an exceptional correlation coefficient of 0.9999. Research indicates that Van der Waals forces and electrostatic relations may facilitate elimination. The EP plant offers a more sustainable treatment for MB-contaminated wastewater, surpassing the performance of conventional adsorbents.

Acknowledgment

The authors express gratitude to everyone who contributed to the successful completion of this work.

Conflict of Interest

None.

Funding

There is no financial support available.

Ethical Clearance

The project was approved by the local ethical committee at University of Baghdad

References

1. Yaqoob AA, Guerrero–Barajas C, Ahmad A, Ibrahim MNM, Alshammari MB. Advanced technologies for wastewater treatment. In Green chemistry for sustainable water purification (eds Shahid-ul-Islam, A.H. Shalla and M. Shahadat); 2023, Ch.8, p. 179-202. https://doi.org/10.1002/9781119852322.ch8.
2. Islam SU, Butola BS. The impact and prospects of green chemistry for textile technology. Woodhead Publishing; 2018.
3. Elnakib HE, Ramsis MM, Albably NO, Vector MA, Weigand JJ, Schwedtmann K, Wober J, Zierau O, Vollmer G, Abadi AH, Ahmed NS. Manipulating estrogenic/anti-estrogenic activity of triphenylethylenes towards development of novel anti-neoplastic SERMs. Int J Mol Sci. 2021; 22(22):12575. https://doi.org/10.3390/ijms222212575.
4. Shindhal T, Rakholiya P, Varjani S, Pandey A, Ngo HH, Guo W, Ng HY, Taherzadeh MJ. A critical review on advances in the practices and perspectives for the treatment of dye industry wastewater.

Bioengineered. 2021; 12(1):70-87. https://doi.org/10.1080/21655979.2020.1863034.
5. Al-Rudaini KA. Adsorption removal of Rhodamine-B dye from aqueous solution using rhamnus stone as low cost adsorbent. Al-Nahrain J Sci. 2017; 20(1):32–41. https://doi.org/10.22401/JNUS.20.1.05.
6. Davidescu S, Murariu G, Dinca L, Vasile D, Crisan V, Cretu R, Georgescu L, Deca S. Growth potential of hybrid black poplar (Populus x Canadensis Moench) in Romania's East Plain. Int J Conserv Sci. 2020;11(3):807–818.
7. Topare NS, Surange S, Chaudhari A, Raut-Jadhav S, Khedkar SV, Bokil SA. Adsorption of Rhodamine-B by using citrus peel powder: influence of operating parameters. J Indian Chem Soc. 2020; 97(11a):2188–2194.
8. Nagham HA, Merza SH. Commercial graphite flakes as an adsorbent of Janus green dye from aqueous solution: Adsorption kinetics and isotherms study. IHJPAS. 2025; 38(4):248-262. https://doi.org/10.30526/38.4.4140.
9. Harja M, Buema G, Bucur D. Recent advances in removal of Congo Red dye by adsorption using an industrial waste. Sci Rep. 2022; 12(1):6087. https://doi.org/10.1038/s41598-022-10093-3.
10. Geetha MP, Pratheeksha P, Subrahmanya BK. Development of functionalized CuO nanoparticles for enhancing the adsorption of methylene blue dye. Cogent Engineering. 2020; 7(1):1783102. https://doi.org/10.1080/23311916.2020.1783102.
11. Zeng XY, Wang Y, Li RX, Cao HL, Li YF, Lü J. Impacts of temperatures and phosphoric-acid modification to the physicochemical properties of biochar for excellent sulfadiazine adsorption. Biochar. 2022; 4(1):14. https://doi.org/10.1007/s42773-022-00143-4.
12. Safari JB, Ushindi VS, Andema FC, Hamuli PM, Irenge EB, Vuangi BM, Zola EN, Baraka BK, Bilamirwa CM, Matabaro VM, Angbongbo FP, Nsabatien V, Zanga J, Metelo EM, Krause RWM, Balčiūnaitienė A, Memvanga PB. Plant-based synthesis of silver nanoparticles using aqueous leaf extracts of *Cinchona calisaya* Wedd. and *Cinchona pubescens* Vahl: Physicochemical characterisation and biological activities. Discover Nano. 2025; 20(1):162. https://doi.org/10.1186/s11671-025-04326-3.
13. Fida M, Iqbal S, Shah M, Fazal T, Ismail B, Rehman HU, Al-Fawzan FF, Elkaeed EB, Pashameah R A, Alzahrani E, Farouk A-E. Mn^{2+} doped cobalt oxide and its composite with carbon nanotubes for adsorption-assisted photocatalytic applications. Sustainability. 2022; 14(24):16932. https://doi.org/10.3390/su142416932.
14. Younas M, Javed T. Exploring the efficiency of sugarcane bagasse (Saccharum officinarum) for decontamination of wastewater containing Congo red dye. J Dispers Sci Technol. 2024; 45(6):1049–1060. https://doi.org/10.1080/01932691.2023.2194400.
15. Sharma R, Satsangee SP, Verma SK. Raw, activated and modified biosorbents for the speciation of CI acid red 2 from aqueous solutions: An adsorption study. Int J Water Resour Environ Eng. 2021; 13(1): 1–19. https://doi.org/10.5897/IJWREE2020.0933.
16. Abouda NA, Jasima BE, Rheimab AM. Methylene Orange dye removal in aqueous solution using synthesized CdO-MnO_2 nanocomposite: Kinetic and thermodynamic studies. Chalcogenide Lett. 2021; 18(5):237–243. https://doi.org/10.15251/CL.2021.185.237.
17. Mahmoud ME, El-Said GF, Ibrahim GA, Elnashar AA. Effective removal of hexavalent chromium from water by sustainable nano-scaled waste avocado seeds: Adsorption isotherm, thermodynamics, kinetics, and error function. Biomass Convers Biorefin. 2024; 14(13):14725-14743. https://doi.org/10.1007/s13399-022-03619-2.
18. Mizhir A, Abdulwahid A, Al-Lami H. Chemical functionalization graphene oxide for the adsorption behavior of bismarck brown dye from aqueous solutions. Egypt J Chem. 2020; 63(5):1679-1696. https://doi.org/10.21608/ejchem.2020.21260.2271.
19. Kadhim AA, Al-Da'amy MA, Kadhim SH. Synthesis of $CuCo_2O_4$-MgO spinel composite as an adsorbent surface for removal of celestine blue B dye. In 4th International Scientific Conference of Engineering Sciences and Advances Technologies. AIP Publishing LLC. 2023; 2830(1):070034. https://doi.org/10.1063/5.0156733.
20. Shaaban AE, Khalil AA, Elewa BS, Ismail M, Eldemerdash UM. A new modified exfoliated graphene oxide for removal of copper (II), lead (II) and nickel (II) ions from aqueous solutions. Egypt J Chem. 2019; 62(10):1823-1849. https://doi.org/10.21608/ejchem.2019.11060.1713.
21. Ismael HA, Mohammad EJ, Atiyah AJ, Kadhim SH, Kahdum KJ. Synthesis and characteristic study of composite zinc oxide and functionalized activated carbon with investigation of its adsorption ability:

A kinetic study. In: IOP Conference Series: Earth and Environmental Science. IOP Publishing. 2021; 12007. http://dx.doi.org/10.1088/1755-1315/722/1/012007.
22. Yan G, Wang P, Li Y, Qin Z, Lan S, Yan Y, Zhang Q, Cheng X. Adsorption-oxidation mechanism of δ-MnO_2 to remove methylene blue. Adsorpt Sci Technol. 2021; 2021:3069392. https://doi.org/10.1155/2021/3069392.
23. Nguyen CH, Tran HN, Fu CC, Lu YT, Juang RS. Roles of adsorption and photocatalysis in removing organic pollutants from water by activated carbon–supported titania composites: Kinetic aspects. J Taiwan Inst Chem Eng. 2020; 109:51–61. https://doi.org/10.1016/j.jtice.2020.02.019.
24. Ngah WSW, Hanafiah M. Adsorption of copper on rubber (Hevea brasiliensis) leaf powder: Kinetic, equilibrium and thermodynamic studies. Biochem Eng J. 2008; 39(3):521–530. https://doi.org/10.1016/j.bej.2007.11.006.
25. Mall ID, Srivastava VC, Agarwal NK, Mishra IM. Removal of congo red from aqueous solution by bagasse fly ash and activated carbon: kinetic study and equilibrium isotherm analyses. Chemosphere. 2005; 61(4):492–501. https://doi.org/10.1016/j.chemosphere.2005.03.065.
26. Lam VT, Dao TT, Nguyen HT, Nguyen DTC, Le HTN, Nguyen HTT, Do ST, Loc HH, Nguyen TD. Process optimization studies of congo red dye adsorption onto magnesium aluminium layered double hydroxide using response surface methodology. Pol J Environ Stud. 2021; 30(1):679–687. https://doi.org/10.15244/pjoes/121048.
27. Dyeoni B, Mbbyn T, Zno A. Adsorption study of Rhodamin B dye on Iraqi bentonite and modified bentonite by nanocompounds TiO_2, ZnO, AL_2O_3 and sodium dodecyl sulfate. Am J Environ Sci. 2013; 9(3):269–279. https://doi.org/10.3844/ajessp.2013.269.279.
28. Lima EC, Hosseini-Bandegharaei A, Moreno-Piraján JC, Anastopoulos I. A critical review of the estimation of the thermodynamic parameters on adsorption equilibria. Wrong use of equilibrium constant in the Van't Hoof equation for calculation of thermodynamic parameters of adsorption. J Mol Liq. 2019; 273:425–434. https://doi.org/10.1016/j.molliq.2018.10.048.
29. Reschützegger T, Salau NPG. Uncertainty impact of isotherm models on liquid-phase adsorption thermodynamics: A Bayesian inference perspective. Clean Chem Eng. 2025; 11:100146. https://doi.org/10.1016/j.clce.2025.100146.
30. Xing Y, Xiao X, Zhao Y, Liu W, Fan Q, Meng G, Qian Y. Thermodynamic and kinetic behaviors of water vapor adsorption on the lower Cambrian over-mature shale and kerogen. Fuel. 2025; 381(Part C): 133560. https://doi.org/10.1016/j.fuel.2024.133560.
31. Kamaci UD, Kamaci M. Cationic dye adsorption on the bioadsorbents based on chitosan and sodium alginate-iron oxide nanoparticles: Kinetic, isotherm and thermodynamic studies. Inorg Chem Commun. 2025; 175:114160. https://doi.org/10.1016/j.inoche.2025.114160.
32. Liu C, Wang W, Wang N, Liu Z, Shen P, Hu J, Shi F. Synthesis of cubic mesoporous silica SBA16 functionalized with carboxylic acid in a one-pot process for efficient removal of wastewater containing Cu^{2+}: Adsorption isotherms, kinetics, and thermodynamics. Microporous Mesoporous Mater. 2025; 382(1-3):113402. https://doi.org/10.1016/j.micromeso.2024.113402.
33. Al-Mahmoud SM. Elimination of crystal violet from aqueous media using *Lagurus ovatus* as a natural adsorbent. ECTJ. 2025; 27(3):219-927. https://doi.org/10.18321/ectj1669.
34. Abbas M, Trari M. Kinetic, equilibrium and thermodynamic study on the removal of Congo red from aqueous solutions by adsorption onto apricot stone. Process Saf Environ Prot. 2015; 98(6):424–436. https://doi.org/10.1016/j.psep.2015.09.015.